Title
A POSITRON TOMOGRAPH WITH 600 BGO CRYSTALS AND 2.6 MM RESOLUTION

Authors
Derenzo, S.E.
Huesman, R.H.
Cahoon, J.L.

Publication Date
1987-10-01

Lawrence Berkeley Laboratory
UNIVERSITY OF CALIFORNIA

Presented at the IEEE Nuclear Science Symposium,
San Francisco, CA, October 19–24, 1987, and to
be published in the Proceedings

A Positron Tomograph with 600 BGO Crystals and 2.6 mm Resolution

S.E. Derenzo, R.H. Huesman, J.L. Cahoon, A.B. Geyer,
W.W. Moses, D.C. Uber, T. Vuletich, and T.F Budinger

October 1987

Donner Biology & Medicine Division

Prepared for the U.S. Department of Energy under Contract DE-AC03-76SF00098

A POSITRON TOMOGRAPH WITH 600 BGO CRYSTALS AND 2.6 MM RESOLUTION*

S.E. Derenzo, R.H. Huesman, J.L. Cahoon, A.B. Geyer,
W.W. Moses, D.C. Uber, T. Vuletich, and T.F. Budinger
Donner Laboratory and Lawrence Berkeley Laboratory,
University of California
Berkeley, CA, 94720

Abstract

We describe the imaging performance of the Donner 600-Crystal Positron Tomograph, a single 60 cm diam ring of 3 mm wide bismuth germanate (BGO) crystals coupled individually to 14 mm phototubes. With a pulse height threshold of 200 keV and a slice thickness of 5 mm, the sensitivity is 7024 events/sec per μCi/ml in a 20 cm cylinder of water. The measured rates for 18 μCi/ml are 95,000 trues/sec plus 20,000 randoms/sec. A 0.3 mm diam ^{22}Na line source near the center of the tomograph has a circular point spread function (PSF) with a full-width at half-maximum (fwhm) of 2.6 mm. At 5 cm from the center the PSF is elliptical with a fwhm of 2.7 mm tangential x 3.2 mm radial. At 10 cm the PSF has a fwhm of 2.8 mm tangential x 4.8 mm radial. Attenuation data are accumulated with a 20 mCi ^{68}Ge orbiting transmission source and 100 million coincident events are collected in 200 sec.

1. Introduction

The Donner 600-Crystal Positron Tomograph was designed to image labeled tracers with 2-3 mm resolution and measure the dynamics of blood flow in the cerebral arteries and the uptake and disappearance of labeled tracers in the brain, especially in small, functionally distinct nuclei. This single ring system has a patient port diameter of 30 cm and was designed to accommodate the human head and neck, and small animals. The design is characterized by independent 3 mm wide detectors for very high spatial resolution and parallel high speed electronics for very high maximum event rates.

A previous report[1] described the initial results of this tomograph and demonstrated a reconstructed spatial resolution of 2.9 mm fwhm. Clam sampling motion was used[2] and the data were reorganized into 1.58 mm wide parallel ray projection bins before reconstruction. In this work we report a spatial resolution of 2.6 mm fwhm using finer 0.79 mm projection bins.

The small animal tomograph of Tomitani *et al.* also uses individual crystal-PMT coupling and has a spatial resolution of 3.5 mm fwhm.[3] Many other tomograph designers couple each small BGO crystal to several larger phototubes and use pulse height ratio logic to determine the crystal of interaction.[4–9] While these designs use fewer phototubes, the low light output of BGO results in statistical fluctuations in the position, and appears to limit the spatial resolution to about 4.5 mm fwhm.

*To be published in *IEEE Trans Nucl Sci* **NS-35**, 1988. This work was supported in part by the U.S. Department of Energy, under Contract No. DE-AC03-76SF00098, and in part by Public Health Service Grant Nos. P01 25840 and R01 CA38086.

2. System Description

2.1 Detectors

Each 3 mm wide BGO crystal[10] is individually coupled to a 14 mm diam R647-01 phototube[11]. The method of coupling the single ring of 600 crystals to five rings of phototubes is described in a previous report.[1] The R647-01 10-stage phototube has a gain of 10^6 at 1000 Volts, a 10–90% risetime of 2 nsec and a single photoelectron transit time spread of 1.2 nsec.[12] See Table 1 for a physical description of the system.

Table 1: Description of the Donner 600-Crystal Tomograph

Number of BGO crystals	600
Detector ring diameter	60 cm
Patient port diameter	30 cm
BGO crystal front face	3 mm x 10 mm
BGO crystal c-c spacing	3.14 mm
Shielding gap width (adjustable)	0 to 10 mm
Number of sampling positions	2
Number of projection data	120,000
Projection bin width	0.79 mm
Timing resolution (first photoelectron)	5 nsec fwhm
Coincidence window width (adjustable)	7 to 12 nsec
Photopeak resolution	20-30% fwhm

2.2 Electronics and Data Acquisition

Each phototube output is sent to a timing discriminator and integrator circuit, then to individual computer-adjustable timing delays and pulse height acceptance windows.[13] A Left/Right (L/R) veto circuit is used to reject events where a pulse height greater than 160 keV is detected in an adjacent crystal.

Each of the 600 crystals is in electronic collimation with the opposing 200 crystals, providing 60,000 crystal pair combinations. High maximum data rates are provided by 45 parallel group coincidence circuits and 4 parallel histogram memory units.[14] Data are accumulated in eight 32,000 16-bit word histogrammers, where each histogram location is incremented for on-time events and decremented for off-time events. During each study the clam position is changed every 2.5 seconds, and two 60,000 element datasets are accumulated. During reconstruction, the datasets for the two clam positions are combined to provide data in 0.79 mm projection bins.[2] The Nyquist limit corresponding to this spatial sampling frequency is 6.4 cycles/cm, which is the highest reconstruction filter cut-off used in this work.

2.3 Orbiting Transmission Source

A 20 mCi ^{68}Ge source[15] orbits in the shielding gap at a radius of 17.8 cm to provide attenuation measurements. The source consists of a 3 mm diam x 5 mm long cylinder of activity sealed in a stainless steel rod. Scattered and random coincidences that do not pass near the source are rejected by the electronics.[16]

3. Imaging Properties

3.1 In-Plane and Axial Resolution

A 0.35 mm diam ^{22}Na line source[15] was used to measure the spatial resolution. The response of a single pair of detectors in the tomograph has a fwhm of 2.5 mm, which is somewhat larger than the 2.0 mm fwhm predicted by combining detector response (1.5 mm), deviations from 180° emission (1.3 mm), and positron range (0.5 mm)[1]. The difference is probably due to small angle scattering from neighboring crystals. The reconstructed image of this source at the exact center of the tomograph has a circular point spread function (PSF) with a full-width at half-maximum (fwhm) of 2.35 mm. When the source is displaced slightly from this special point, the PSF remains circular but the fwhm increases to 2.6 mm. As the line source is moved further from the tomograph center, crystal penetration causes the radial component of the PSF to increase, resulting in an elliptical shape (Table 2, Figure 1). The measured resolutions in Table 2 are independent of both the lower pulse height threshold (in the range from 100 to 350 keV) and whether the L/R veto circuit is ON or OFF.

Table 2: Measured In-Plane and Axial Resolution

Distance from center	fwhm (mm)	fwtm (mm)
Reconstructed In-plane image resolution[a]:		
at exact center	2.35 x 2.35[b]	4.6 x 4.6
1 cm	2.6 x 2.7	5.0 x 5.0
5 cm	2.7 x 3.2	5.1 x 5.9
10 cm	2.8 x 4.8	5.3 x 8.6
14.4 cm	3.1 x 7.7	5.5 x 13.8
Axial response[c]:		
0 cm	5.7	9.5
5 cm	5.8	9.4
10 cm	6.1	9.5
14.4 cm	6.3	9.7

[a]0.35 mm diam line source parallel to the tomograph axis. Data reconstructed with a filter cutoff at 6.4 cycles/cm.
[b]tangential × radial
[c]0.35 mm diam line source perpendicular to the tomograph axis.

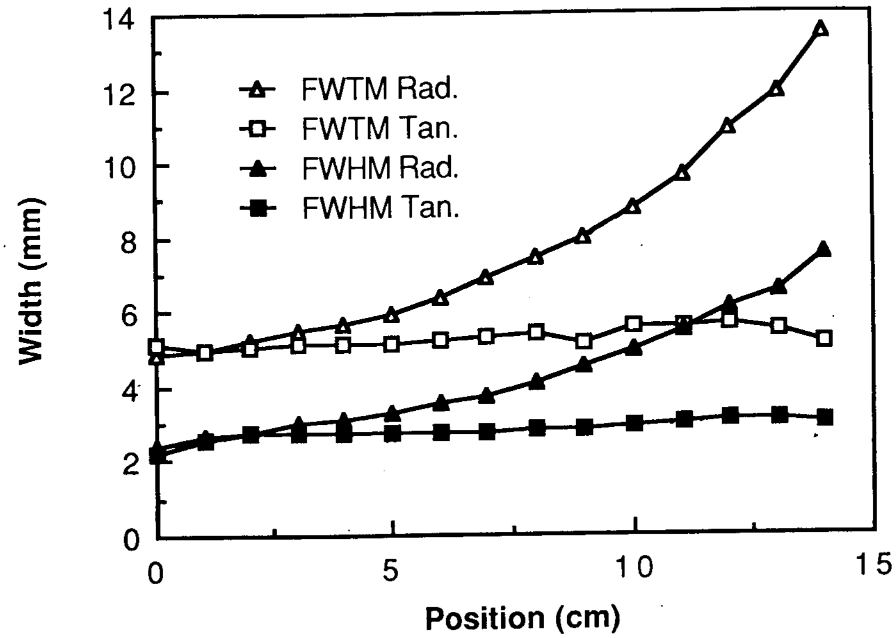

Figure 1: Full-width at half-maximum (fwhm) and full-width at tenth-maximum (fwtm) of the of the Radial (Rad.) and Tangential (Tan.) components of the reconstructed image of a 0.35 mm diam ^{22}Na wire as a function of the distance to the center of the tomograph. Clam sampling was used and the images were reconstructed from 0.79 mm projection bins.

3.2 Sensitivity

The sensitivity of the tomograph was measured with a 20 cm diam cylinder of ^{68}Ga solution. The sensitivity depends on the lower pulse height threshold and the L/R veto (Table 3). At our standard pulse height threshold of 200 keV and with L/R veto OFF, the sensitivity is 7,024 events/sec per µCi/ml.

Lowering the lower pulse height threshold increases the total event rate, but it also increases the prompt scatter and random backgrounds (Table 4). To explore this tradeoff, we imaged a 6 mm diam line source of ^{68}Ga on the ring axis and separately measured image events (true coincidences passing within 16 mm of the source center), prompt scatter events (true coincidences passing farther than 16 mm from the source center), and random events (coincidences in the off-time window) in the parallel ray projection data. The effective event rate is defined as the image event rate times the image fraction, which represents the statistical value of each event after background subtraction. The effective image rate is optimized at 200 keV, indicating that unscattered annihilation photons that are detected by a single Compton scatter are an important source of image information.

The upper level threshold did not affect the data at low and moderate rates because even when using ^{22}Na, which has a coincident 1.3 MeV gamma ray, the pulse height spectrum of coincident events does not extend above the 511 keV photopeak.

Table 3: Event rates for 1 μCi/ml in a 20 cm water cylinder[a]

Lower Threshold (keV)	L/R Veto	True Event Rate[b]	Random Event. Rate[c]	Total Event Rate
350	OFF	4,662	36	4,699
300	OFF	5,498	49	5,546
250	OFF	6,384	63	6,447
200	OFF	7,024	79	7,103
150	OFF	7,169	95	7,264
100	OFF	7,141	115	7,256
350	ON	4,398	34	4,432
300	ON	5,105	45	5,150
250	ON	5,855	58	5,913
200	ON	6,503	73	6,576
150	ON	6,822	90	6,912
100	ON	6,975	111	7,086

[a]Data taken with 7 to 10 μCi ^{68}Ga per ml and converted to 1 μCi/ml of pure positron emitter.
[b]Determined by subtracting the off-time Coincidence Rate (randoms) from the on-time Coincidence Rate (image + scatter + random).
[c]Event Rate in the off-time coincidence window.

Table 4: Event rates for a 1 mCi per axial cm line source in 20 cm water[a]

Lower Threshold (keV)	L/R Veto	Image Event Rate[b]	Scatter Event Rate[c]	Random Event Rate	Total Event Rate[d]	Image Fraction[e]	Effective Event Rate[f]
350	OFF	13,587	1,295	882	15,764	0.86	11,711
300	OFF	15,859	1,762	1,308	18,928	0.84	13,287
250	OFF	18,165	2,245	1,878	22,287	0.82	14,804
200	OFF	19,774	2,671	2,682	25,127	0.79	15,562
150	OFF	20,119	2,980	3,784	26,882	0.75	15,057
100	OFF	19,762	3,164	5,520	28,446	0.69	13,729
350	ON	13,226	1,324	863	15,414	0.86	11,350
300	ON	15,322	1,721	1,246	18,289	0.84	12,836
250	ON	17,115	2,137	1,779	21,031	0.81	13,929
200	ON	18,925	2,556	2,550	24,031	0.79	14,904
150	ON	19,421	2,851	3,727	26,000	0.75	14,507
100	ON	19,531	3,127	5,534	28,192	0.69	13,530

[a]Data taken using 0.20 to 0.25 mCi ^{68}Ga per axial cm and converted to 1 mCi per axial cm of pure positron emitter.
[b]Events in the projection data within 16 mm of the line source.
[c]Events in the projection data farther than 16 mm from the line source (i.e. coincident scatter background)
[d]Total for the on-time coincidence window. In addition, an independent Random Event Rate is recorded in the off-time window.
[e]Computed as (Image Event Rate)/(Total Event Rate)
[f]Computed as (Image Event Rate) × (Image Fraction)

3.3 Phantom Images

A 20 cm diam, six-compartment phantom was constructed to test the quantitative accuracy of the tomograph, its electronics, and the reconstruction algorithm. The compartments were filled with approximately 0, 1, 2, 3, 4, and 5 units of 2.90 mCi of ^{68}Ga and imaged (Figure 2). The reconstructed activity in each compartment has an excellent linear relationship with the activity in each compartment, and the zero activity intercept corresponds to 0.07 units of activity, demonstrating the subtraction of the prompt scatter background in the reconstruction process (Table 5, Figure 3).

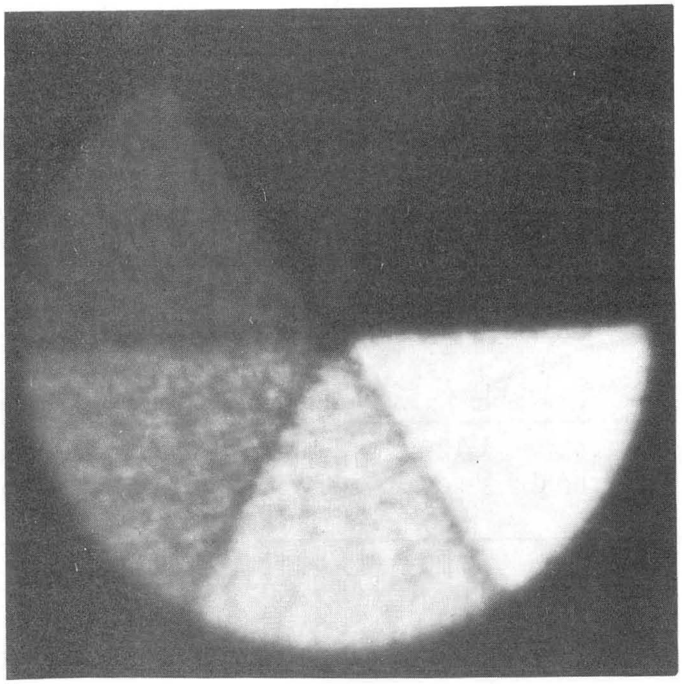

Figure 2: Image of 57 million ^{68}Ga events in a phantom with six pie-shaped compartments. Approximately 0, 1, 2, 3, 4, and 5 units of activity were placed in the respective compartments. The reconstruction filter had a high frequency rolloff that dropped from 0.90F at 0.7 cycles/cm to 0.10F at 3.1 cycles/cm, where F is the spatial frequency.

Table 5: Activity in Compartments vs Reconstructed Activity

Compartment	A=activity (µCi/ml)	Reconstructed Activity[a]	Fractional Deviation[b]
1	0.00	23	+0.006
2	2.98	346	–0.020
3	6.01	704	–0.012
4	8.61	1,052	+0.042
5	11.50	1,350	–0.001
6	14.40	1,674	–0.016

[a]arbitrary units
[b](reconstructed activity – best straight line fit)/(average of the 6 compartments)

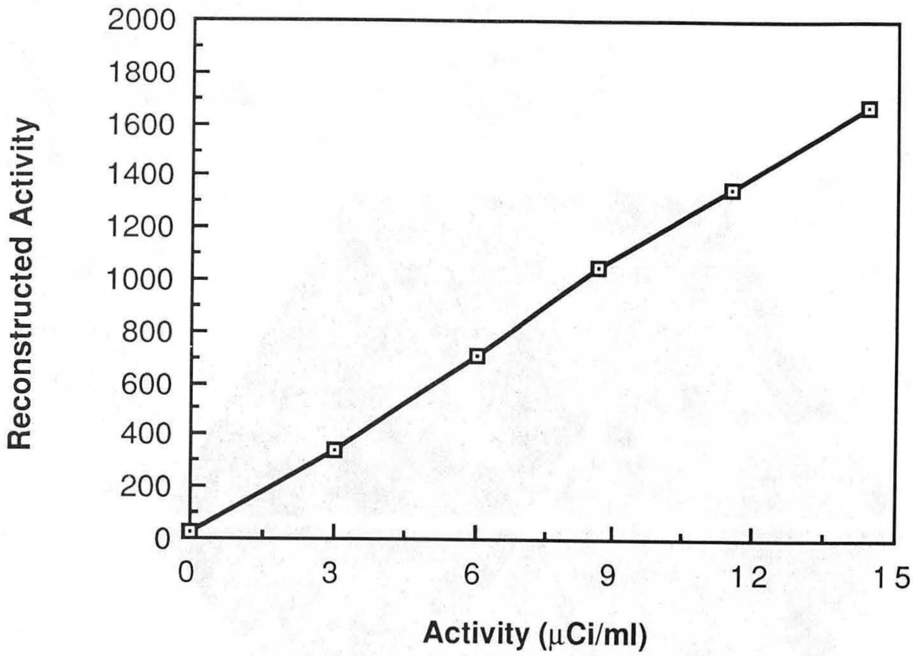

Figure 3: Correspondence between the measured activity in each compartment of the pie-shaped phantom of Figure 2 and the reconstructed activity. The reconstructed activity is nearly zero in the compartment with zero activity, demonstrating the subtraction of the prompt scatter background in the reconstruction process.

Our previously described hot-spot phantom is easily resolved with this high resolution tomograph and it was necessary to design and build a phantom with much finer structures.[1] Figure 4 shows an image of 45 million ^{18}F events using this phantom, and Figure 5 shows the reconstructed intensity profiles along each row of hot spots.

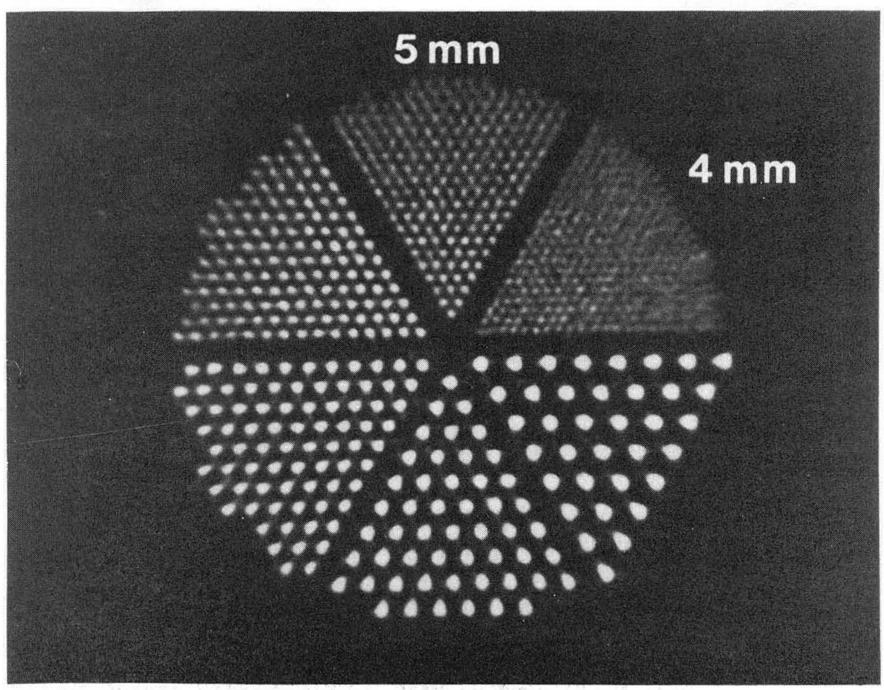

Figure 4: Image of 45 million ^{18}F events of a 20 cm diam high resolution hot spot phantom (Figure 4) taken with the Donner 600 crystal Positron Tomograph using clam sampling and 0.79 mm projection bins. The reconstruction filter had a high frequency rolloff that dropped from 0.90F at 3.1 cycles/cm to 0.10F at 3.7 cycles/cm, where F is the spatial frequency.

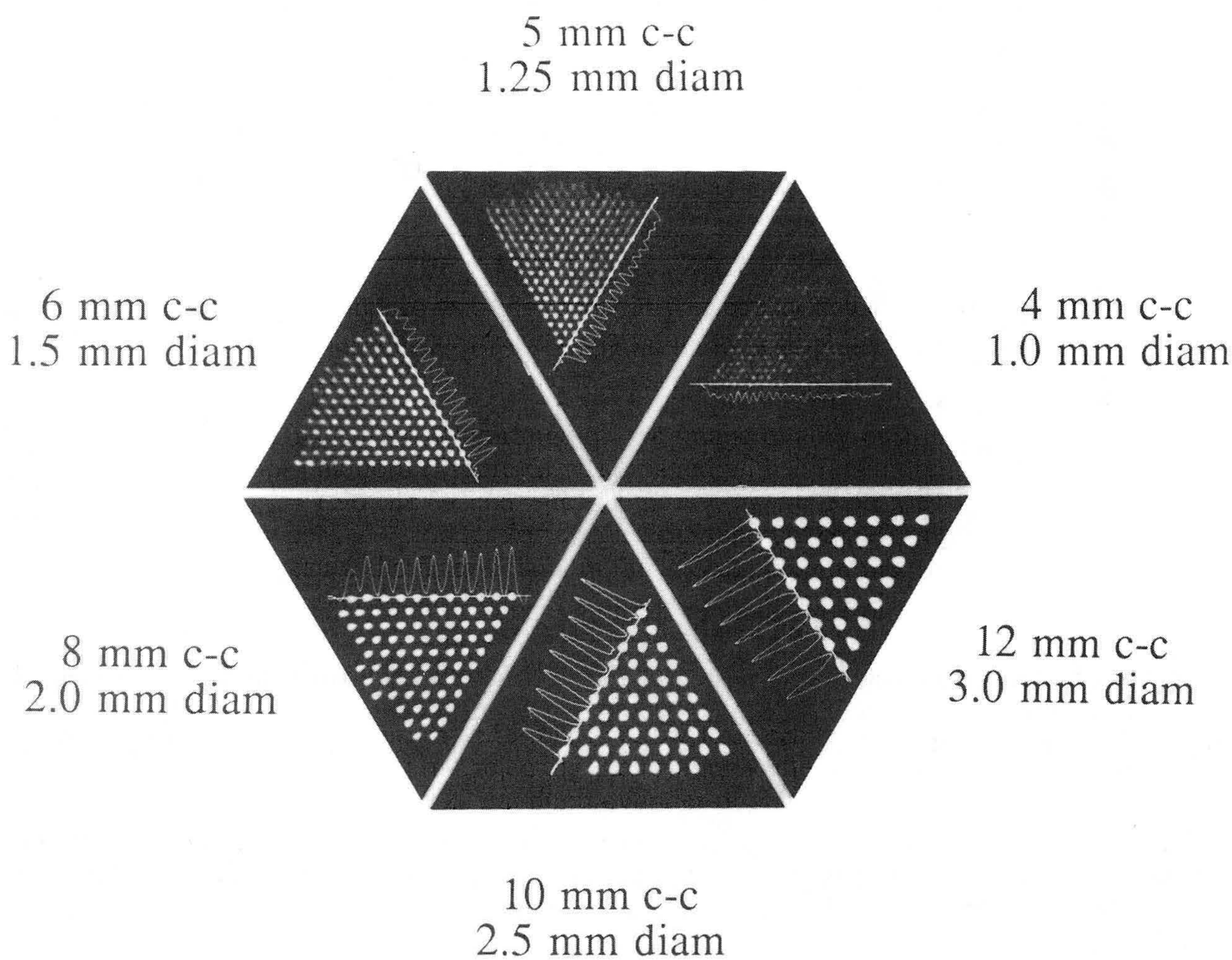

Figure 5: Profiles through the rows of hot spots in the reconstructed image of Figure 4. Radial elongation in outer regions of phantom is due to crystal penetration for off-axis rays.

To visualize the effect of positron range on the image quality of a high resolution positron tomograph, a 37-point phantom (Figure 6) was imaged with ^{18}F (Figure 7, $E_{max} = 0.64$ MeV), ^{68}Ga (Figure 8, $E_{max} = 1.90$ MeV), and ^{82}Rb (Figure 9, $E_{max} = 3.35$ MeV). The positron range distribution is sharply peaked[17] and retains a significant amount of information at the high spatial frequencies[18]. As a result, the finer details in the ^{68}Ga and even the ^{82}Rb image can be seen, although the contrast is severely reduced.

3.4 Attenuation Measurements

The event rate for the 3 mm diam, 5 mm long, 20 mCi orbiting transmission source in air is 750,000 coincident events/sec, after rejecting the prompt scatters and random events that do not pass through the source. When a 20 cm diam cylinder of water is placed in the tomograph, this rate drops to 490,000 coincident events/sec.[16]

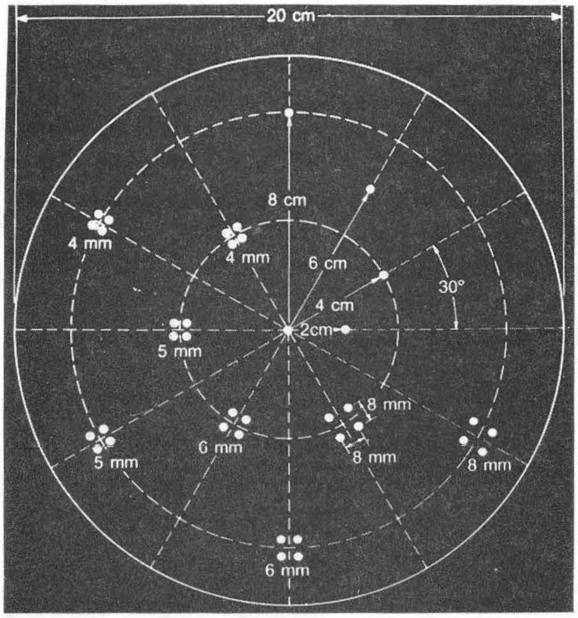

Figure 6: Sketch of a 37-point hot spot phantom formed by drilling channels in a solid 20 cm cylinder of plexiglass.

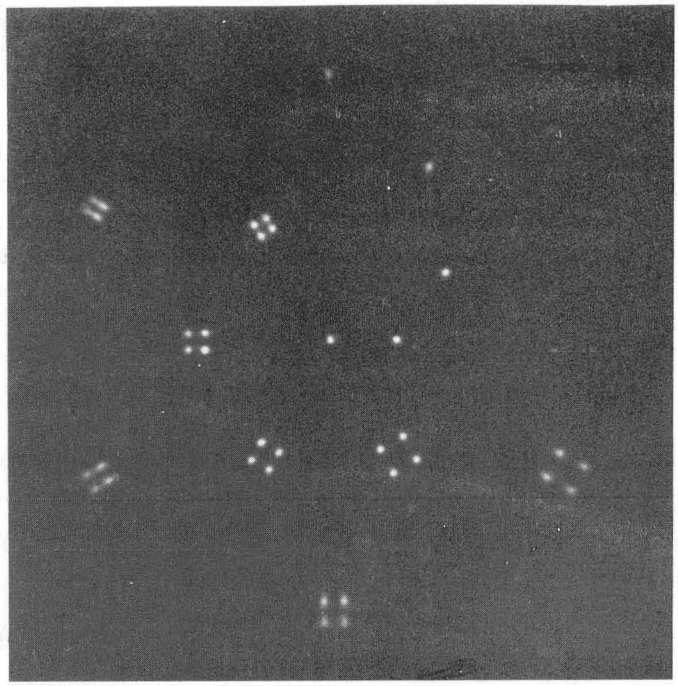

Figure 7: 22 million ^{18}F events in the 37 point hot spot phantom. The reconstruction filter had a sharp high frequency cut off at 6.4 cycles/cm.

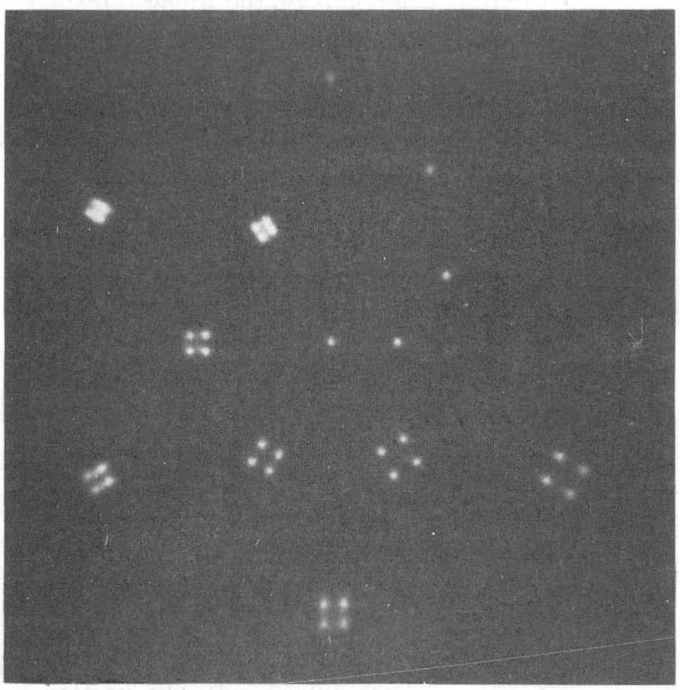

Figure 8: 13 million ^{68}Ga events in the 37 point hot spot phantom. The reconstruction filter had a sharp high frequency cut off at 6.4 cycles/cm.

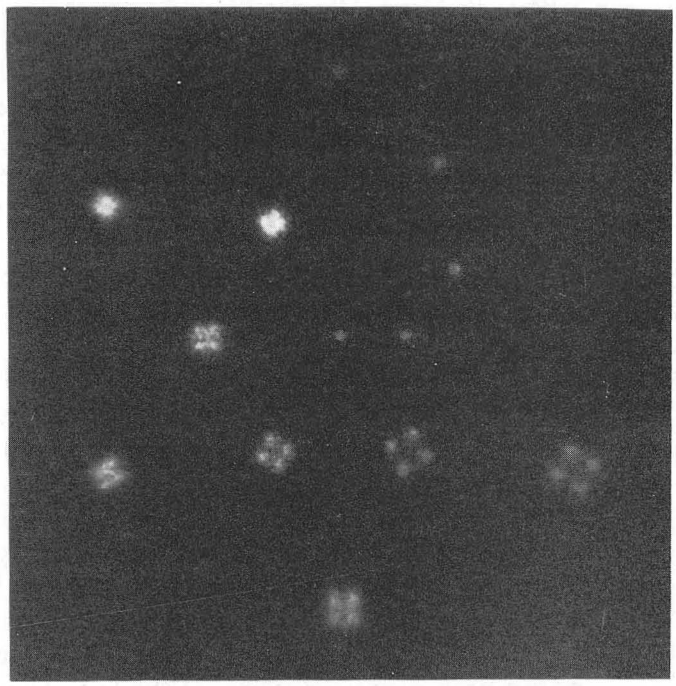

Figure 9: 7 million ^{82}Rb events in the 37 point hot spot phantom. The reconstruction filter had a sharp high frequency cut off at 6.4 cycles/cm.

4. Future Developments

Usually in positron emission tomography, emission images can be taken only of sections that have been transmission scanned previously. To eliminate this requirement and be able to image any section at any time, even after the patient has moved on the tomograph bed, we and others[19] are investigating the possibility of making attenuation measurements after the positron activity has been administered. This is possible because the 20 mCi orbiting transmission source provides a much higher event rate than a typical emission study, and the rotating transmission mask rejects almost all emission events. The subtraction of the remaining emission data increases the statistical noise by only a small amount.

We are developing detectors and electronics for multi-layer ultra-high resolution positron tomography using a combination of photomultiplier tube and silicon photodiode readout.[20] A group of crystals is coupled to a phototube which provides timing and pulse height information for that group, and each crystal is coupled individually to a position-sensitive photodiode which provides the pulse height and depth of interaction in the crystal.

5. Conclusions

(1) The reconstructed point spread function has a circular fwhm of 2.6 mm near the center and an elliptical fwhm of 2.8 mm x 4.8 mm at 10 cm from the center.

(2) The axial resolution is 6 mm fwhm.

(3) Spatial resolution is unaffected by changing lower threshold or by using the L/R veto.

(4) The sensitivity as measured with a 20 cm diam water cylinder depends on the lower threshold and to a lesser extent on the use of the LR veto. With a threshold of 200 keV and the L/R veto off, the sensitivity is 7,024 events/sec per µCi/ml.

(5) The lower pulse height threshold that provides the best effective sensitivity for a line source with 1 mCi per axial cm in a 20 cm cylinder is 200 keV. This takes under consideration both the image events and the statistical noise introduced by the scatter and random background events.

(6) The reconstructed quantitation is excellent, as demonstrated by a multi-compartment phantom.

(7) Many parallel detectors and parallel high speed electronics permit very high event rates, even when using a slow scintillator such as BGO.

Acknowledgements

We thank B. Leskovar, C.C. Low, B. Turko, and G. Zizka for contributions to the design and development of the front-end electronics, John Berkowitz for the mechanical design of the gantry, X. Xie for contributions to detector design, and K. Brennan, K. Bristol, M. Colina, M. Morimoto, and J. Twitchell for numerous contributions.

This work was supported in part by the Director, Office of Energy Research, Office of Health and Environmental Research of the U.S. Department of Energy, under Contract No. DE-AC03-76SF00098, and in part by Public Health Service Grant Nos. P01 HL25840 and R01 CA38086 awarded by the National Heart Lung and Blood and National Cancer Institutes, Department of Health and Human Services.

References

[1] Derenzo SE, Huesman RH, Cahoon JL, Geyer A, Uber D, Vuletich T, and Budinger TF: Initial results from the Donner 600 crystal positron tomograph. *IEEE Trans Nucl Sci* **NS-34:** 321-325, 1987

[2] Huesman RH, Derenzo SE and Budinger TF: A two-position sampling scheme for positron emission tomography. In Nuclear Medicine and Biology, Raynaud C, ed., Pergammon Press, New York, Vol I, pp 542-545, 1983.

[3] Tomitani T, Nohara N, Morayama H, et al: Development of a high resolution positron CT for animal studies. *IEEE Trans Nucl Sci* **NS-32:** 822-825, 1985

[4] Burnham CA, Bradshaw J, Kaufman D, et al: Design of cylindrical shaped scintillation camera for positron tomographs. *IEEE Trans Nucl Sci* **NS-32:** 889-893, 1985

[5] Casey ME and Nutt R: A multicrystal two dimensional BGO detector system for positron emission tomography. *IEEE Trans Nucl Sci* **NS-33:** 460-463, 1986

[6] Yamamoto S, Miura S, and Kanno I: A BGO detector using a new encoding scheme for a high resolution positron emission tomograph. *Nucl Instr Meth* **A248:** 557-561, 1986

[7] Eriksson L, Bohm C, Kesselberg M, Holte S, Bergström, and Litton J: Design studies of two possible detector blocks for high resolution positron emission tomography of the brain. *IEEE Trans Nucl Sci* **NS34:** 344-348, 1987

[8] Min HB, Ra JB, Jung KJ, Hilal SK, and Cho ZH: Detector identification in a 4x4 BGO crystal array coupled to two dual PMTs for high resolution positron emission tomography. *IEEE Trans Nucl Sci* **NS34:** 332-336, 1987

[9] Wong WH, Jing M, Bendriem B, Hartz R, Mullani N, Gould L, and Michel C: A slanting light-guide analog decoding high resolution detector for positron emission tomography camera. *IEEE Trans Nucl Sci* **NS34:** 280-284, 1987

[10] Manufactured by Harshaw Chemical Co., Solon, Ohio

[11] Manufactured by Hamamatsu TV Co., Ltd., Hamamatsu, Japan

[12] Lo CC and Leskovar B: Performance studies of Hamamatsu R647-01 photomultiplier. *IEEE Trans Nucl Sci* **NS-31:** 413-416, 1987

[13] Turko BT, Zizka G, Lo CC, Leskovar B, Cahoon JL, Huesman RH, Derenzo SE, Geyer AB, and Budinger TF: Scintillation photon detection and event selection in high resolution positron emission tomography. *IEEE Trans Nucl Sci* **NS-34:** 326-331, 1987

[14] Cahoon JL, Huesman RH, Derenzo SE, et al: The electronics for the Donner, high resolution 600-crystal positron tomograph. *IEEE Trans Nucl Sci* **NS-33:** 570-574, 1986

[15] Fabricated by Isotope Products Laboratories, Burbank, CA

[16] Huesman R, Derenzo S, Cahoon J, Geyer A, Uber D, Vuletich T, and Budinger T: Orbiting transmission source for positron tomography. Submitted to *IEEE Trans Nucl Sci* **NS-35** (1988)

[17] Derenzo, SE: Precision measurement of annihilation point spread distributions for medically important positron emitters. In: *Positron Annihilation*, Hasiguti RR and Fujiwara K, eds, pp 819-823, The Japan Institute of Metals, Sendai, Japan, 1979

[18] Derenzo SE: Mathematical removal of positron range blurring in high resolution tomography. *IEEE Trans Nucl Sci* **NS-33:** 565-569, 1986

[19] Daube-Witherspoon ME, Carson RE, and Green MV: Post-injection transmission attenuation measurements for PET. Submitted to *IEEE Trans Nucl Sci* **NS-35** (1988)

[20] Derenzo SE: Initial characterization of a BGO-silicon photodiode detector for high resolution PET. *IEEE Trans Nucl Sci* **NS-31:** 620-626, 1984

LAWRENCE BERKELEY LABORATORY
TECHNICAL INFORMATION DEPARTMENT
UNIVERSITY OF CALIFORNIA
BERKELEY, CALIFORNIA 94720